Annals of Arid Zone 35(3) : 187-213, 1996

Laboratory Simulation of Aeolian Sand Transport and Physical Modeling of Flow Around Dunes

Bruce R. White
Mechanical and Aeronautical Engineering Department,
University of California Davis, Davis, CA 95616, U.S.A.

Abstract : This paper discusses the possibilities of laboratory simulation of large-scale flow around dunes, both with and without saltation, and the study of the physics of the small-scale particle motion occurring on a sand surface composed of like-moveable particles. Physics of the atmospheric boundary layer are presented in the context of laboratory applications. The governing equations of fluid and/or particle motion are discussed and analyzed for applications in laboratory testing. The most important similitude parameters, as applied to wind-tunnel requirements for conservation of mass, momentum, energy, and the boundary conditions are presented and discussed. Key findings and results are that: i) in general, flow around a dune or multiple dunes with saltation present cannot be accurately simulated in wind tunnels; ii) flow field around all or part of a full-scale dune can be simulated marginally in a wind tunnel, provided "large" model scales and "reasonably high" wind-tunnel speeds are used (the conditions of "large" model scales and "reasonably high" speeds are specified within the text); and, iii) it is possible to accurately replicate the process of saltation in wind tunnels provided appropriate similitude and independence criteria of Reynolds and Froude numbers are observed. Limited laboratory and wind-tunnel studies are cited.

Key words : Dunes, sand transport, simulation, modeling, wind tunnel.

The physical modeling of dunes and associated surface features occurring in arid regions of the earth has been scarce due to the difficulties in achieving reasonable simulation. The majority of modeling experiments that have been conducted used boundary-layer-type wind tunnels since they reasonably simulate the surface-layer flow of the atmospheric boundary layer (ABL) for neutral stability conditions. The surface layer of the ABL varies in height as it is a function of surface roughness, z_o, and the wind speed above the ABL which is called the geostrophic wind, V_g. Also effecting flow in the surface layer is the stability of the atmosphere, which is usually presented in terms of the Monin-Obukhov stability length, L, and other parameters to a lesser degree. Typical heights of the surface layer range from tens of meters to an upper limit height of about 100 meters.

The ABL surface layer has several unique characteristics that lend themselves nicely to be modeled in an atmospheric boundary-layer wind tunnel (ABLWT) or environmental wind tunnel. An environmental wind tunnel differs from an ABLWT in the sense that it usually has capabilities of varying the temperature profiles within its test section, by either heating of cooling the floor or the ceiling. The surface layer is two-dimensional in nature and for the most part is not complicated with the three-dimensional Coriolis effects that result in the so-called turbulent Ekman spiral layer. Since a wind tunnel cannot model this three-dimensional effect, this limits the ABLWT simulation to the lower 50 to 100 meters of

the ABL. The turbulent Ekman spiral three-dimensional effects primarily occur above the surface layer and below the upper edge of the ABL. This lack of modeling ability is of little consequence except for simulation of large-scale earth features such as large dune fields greater than a few kilometers in length or greater than 100 meters high.

The second unique feature of the ABL surface layer is that the mean velocity profile and the turbulence intensity profile above the surface can be simulated in the ABLWT and environmental wind tunnel, respectively. Additionally, the total kinetic energy of the turbulent motion, which may be regarded as a sum of contribution from various sized eddies of the flow, is given by a turbulent energy spectrum function, $E(\kappa)$, where κ is the wave number defined as $\kappa = 2\pi/\lambda$, where λ is the wave length of individual eddies. From dimensional analysis it can be shown that

$$E(\kappa) = \alpha \varepsilon^{2/3} \kappa^{-5/3} \quad (1)$$

for the spectra in the inertial subrange of isotropy turbulence such as in the surface layer of the ABL. Here α is a constant (equal to about 1.5) and ε is the rate of energy dissipation. In ABLWT, with sufficient fetch (10 to 20 meters in length), the naturally developing flow over the rough floor of the tunnel will simulate the key features of Equation (1).

The Atmospheric Boundary Layer

One of the basic features of the ABL is its turbulence. The most unique feature and basic nature of turbulent motion is that flow parameters are not constant with respect to time at a fixed point in space, but fluctuate through a wide range of frequencies. The mean temperature and velocity profiles are directly affected by the random-like fluctuation of temperature and velocity. Turbulent flow has long been thought of as a three-dimensional flow with a random-like distribution of vortical eddies superimposed on the main flow.

Classical studies of the turbulent boundary layer are extensive (Monin and Yaglom, 1965; Lumley and Panofsky, 1964; and many others). From experiments conducted by Nikuradse (1932, 1933) on flow in rough-walled pipes, Schlichting (1968) and Sutton (1953), with others, presented and discussed the logarithmic velocity profile law. For the case of a neutral stratified ABL, Bagnold (1941) observed that it also obeys the logarithmic law, i.e.,

$$\frac{\bar{u}(z)}{u_*} = \frac{1}{k} \log \left(\frac{z}{z_o} \right) \quad (2)$$

where, $\bar{u}(z)$ is the time averaged velocity which is a function of height, z; u_* is the friction speed, k is von Kármán's universal constant; z is the height above the surface; and z_o denotes the equivalent-surface-roughness height.

The two-dimensional turbulent boundary layer has been shown by Clauser (1956) to have a double structure. The double structured layer consists of an inner (or "surface") layer and an outer (or "defect") layer. The ABL also has a similar type of double structure. The ABL's surface is like the two-dimensional inner layer, while the outer layer is three-dimensional in nature. The three-dimensionality of the ABL outer layer is caused by a balance of the rotation force of the earth (or planet) and frictional force. The resultant force caused by the rotation is called the Coriolis force. The Coriolis force causes the direction of the mean wind in the outer portion of the planetary layer to turn to the right (in the northern hemisphere) with increasing height. The three-dimensional turbulent ABL also is known as an "Ekman Spiral" or "Ekman Layer" (mentioned earlier), named after Ekman (1905) who first discovered the phenomenon and used it in a discussion of wind-generated ocean currents

on a rotating earth. The rate of turning with height of the Ekman layer depends on the distribution of eddy viscosity and fluid density.

Fundamental Principles of Laboratory Simulation

An important application in the physical modeling of the ABL is laboratory simulation by use of wind tunnels. Great insight and understanding of the physical flow can be ascertained if correct similitude principles are obeyed. A review of their criteria follows. The review is restricted to the lower portion of the turbulent boundary layer which is relevant to the present problem of sand dune formation, surface modification by winds, and sand movement by aeolian processes.

In order to properly model the lower portion of the ABL in a wind tunnel, certain necessary conditions must be met. In the 1960s, Cermak *et al.* (1966), Hidy (1966), and McVehil *et al.* (1967) demonstrated that wind tunnels can successfully model the ABL's surface layer. Many others have used modeling of the ABL by laboratory simulation with various degrees of success (Halitsky, 1969; Plate and Ouraishi, 1965; Cermak, 1971). The Monin and Obukhov (1954) similarity theory offers a solid theoretical foundation on which to base modeling a stably stratified ABL (Arya and Plate, 1969).

The study of surface (or inner) layer has been extensive. As a result many studies have been conducted; good discussions of these are given in Monin and Yaglom (1965), Lumley and Panofsky (1954), and a basic review of the atmospheric layer is presented in Monin (1970). From the similarity theory of Monin and Obukhov (1954), the surface layer can be modeled if planar homogeneity exists. A detailed review of the implications of homogeneity to the similarity theory is given by Calder (1966). Exact modeling of the entire ABL in detail is not possible. However, by relaxing these requirements and deleting certain non-essential similitude parameters that need not be strictly matched, one can obtain a reasonable laboratory simulation of atmospheric flows.

Equations of motion

The similarity criteria can be obtained from the equations of motion for a particular flow problem by non-dimensionalizing the equations. As a result the non-dimensional equations will yield the governing similitude parameters as coefficients of the individual terms of the normalized equations of motion. Thus, by matching the non-dimensional coefficients of the equations of motion (between laboratory and full-scale) the same physical processing of the full-scale flow should be simulated exactly in the laboratory.

If horizontal and vertical geometry are maintained it will result in an invariant non-dimensional transformation of the conservation of mass (we use cartesian tensor notation and Einstein summation convention):

$$\frac{\partial \bar{u}_i}{\partial x_i} = o \text{ and } \frac{\partial \rho}{\partial t} + \frac{\partial \left(\rho \bar{u}_i\right)}{\partial x_i} = 0 \qquad (3a, b)$$

Non-dimensionalization of the time-averaged momentum equation yields the criteria for dynamic similarity. The time-averaged momentum equation is

$$\frac{\partial \bar{u}_i}{\partial t} + \bar{u}_j \frac{\partial \bar{u}_i}{\partial x_j} + 2\varepsilon_{ijk}\Omega_j \bar{u}_k \qquad (4)$$

$$= -\frac{1}{\rho_o}\frac{\partial \bar{p}}{\partial x_i} - \frac{\Delta T}{T_o} g \delta_{i3} + \nu_o \frac{\partial^2 \bar{u}_i}{\partial x_j} + \frac{\partial \left(\overline{-u_j u_i}\right)}{\partial x_j}$$

where, the dependent variables are represented by mean quantities (represented by the bar over the variable) and fluctuating values (no bar over the variable). The Boussinesq density approximation is made and therefore limits the application of the equation to flows where $\Delta T << T_o$. Note $\bar{p}$ is the deviation of pressure from the atmospheric pressure associated with ρ_o. Using the following non-dimensionalization of variables,

$$\hat{u}_i = \bar{u}_i/u_o \; ; \; \hat{u}'_i = u'_i/u_o \; ; \; \hat{x}_i = x_i/L_o$$
$$\hat{t} = tu_o/L_o \; ; \; \hat{\Omega}_j = \Omega_j/\Omega_o \; ; \; \hat{\bar{p}} = \bar{p}/\rho_o u_o^2$$
$$\Delta\hat{T} = \Delta T/(\Delta T)_o \; ; \; g = g/g_o \qquad (5a\text{-}5h)$$

leads to the non-dimensionalized momentum equation which is given as:

$$\frac{\partial \hat{u}_i}{\partial t} + \hat{u}_j \frac{\partial \hat{u}_i}{\partial x_j} + \underbrace{\left[\frac{L_o \Omega_o}{u_o}\right]}_{1} 2\varepsilon_{ijk} \hat{\Omega}_j \hat{u}_k =$$

$$= \frac{\partial \hat{\bar{p}}}{\partial x_i} - \underbrace{\left[\frac{\Delta T L_o g_o}{T_o \; u_o^2}\right]}_{2} \Delta\hat{T} g \delta_{i3}$$

$$+ \underbrace{\left[\frac{\nu_o}{u_o l_o}\right]}_{3} \frac{\partial^2 \hat{u}_i}{\partial x_k \partial x_k} + \frac{\delta(-\overline{\hat{u}'_i \hat{u}'_j})}{\partial x_j} \qquad (6)$$

Three similitude parameters appear as coefficients for the non-dimensionalized terms of the momentum equation. In order to maintain proper dynamic similarity the three similitude parameters should be matched to their full scale values in laboratory simulation. These three parameters are known as:

1. Rossby number; $R_o = u_o/L_o\Omega_o$ (7)

2. Bulk Richardson number ;

$$R_i = \left[(\Delta T)_o / T_o\right]\left[L_o g_o / u_o^2\right] \qquad (8)$$

3. Reynolds number; $R_e = u_o L_o/\nu_o$ (9)

The Rossby number is associated with the ratio of advective (or local acceleration) to the Coriolis effect caused by the earth's rotation, Ω_o. In order to simulate the entire ABL and accurately model three-dimensional Ekman layers as well as the surface layer, it would be necessary to rotate the entire wind tunnel at constant speed. Caldwell (1972) and Howroyd and Slawson (1975) present laboratory studies of this situation. However, it is relatively impractical to use a rotating wind tunnel and for the most part, both in the atmosphere and in the non-rotating wind tunnel, the mean velocity profile is very logarithmic over the lower 10 to 15% of the boundary layer (Tennekes, 1973).

A wind tunnel with sufficient fetch will produce a boundary-layer height of about one meter, suggesting that the lower 10 to 15 cm may be used to simulate the surface layer of the ABL, in which the longitudinal velocity spectrum in the inertial subrange would be accurately modeled (Equation 1). Therefore, Rossby number effects may be ignored if laboratory testing is contained in the lower 10 to 15% of the boundary-layer height. This also imposes a practical upper limit on longitudinal length that may be modeled of a few kilometers (i.e., length in the flow direction). Thus, full-scale fetches of only a few kilometers may be modeled in the laboratory.

The second non-dimensional parameter is the bulk Richardson number which represents buoyant to inertial forces. Small values of R_i suggest that inertial forces are dominant. Therefore, thermal effects become important for R_i values equal to or greater than unity. Thus, if the atmospheric flow were of neutral stability, the R_i would be zero and this situation would be easily simulated in the laboratory by isothermal flow.

The third parameter is the Reynolds number and perhaps the most significant one. The Reynolds number is the ratio of inertial to viscous forces. Typical laboratory scale reductions result in model Reynolds numbers that may be several orders of magnitude less than those found in the field. If strict adherence to a Reynolds number criterion were required, almost no field cases could be modeled. Fortunately, there exists a phenomenon called Reynolds number independence, that, in the absence of Rossby and bulk Richardson number effects, states scaled model flows will be dynamically similar to the full-scale case

if the Reynolds number is equal to or greater than the minimum independence value (Townsend, 1956). Townsend states that "geometrically similar flows are similar at all sufficiently high Reynolds numbers." He called this Reynolds-number similarity. Today, there exists a large body of experimental studies validating his theory. If it were not for the principle of Reynolds number independence very little physical modeling could be carried out.

The time averaged conservation of energy equation, neglecting conduction, radiation and pressure terms, is,

$$\frac{\partial \overline{T}}{\partial t}+\overline{u}_i\frac{\partial \overline{T}}{\partial x_i}=\left[\frac{\kappa_o}{\rho_o c_{po}}\right]\frac{\partial\left(-\theta' \overline{u'_i}\right)}{\partial x_i}+\frac{\overline{\phi}}{\rho_o c_{po}} \tag{10}$$

where ϕ is the dissipation friction. After non-dimensionalizing the energy equation, it becomes:

$$\frac{\partial \hat{T}}{\partial \hat{t}}+\hat{u}_i\frac{\partial \hat{T}}{\partial \hat{x}_i}=\underbrace{\left[\frac{\kappa_o}{\rho_o c_{po} v_o}\right]}_{4}\left[\frac{v_o}{L_o u_o}\right]\frac{\partial^2 \hat{T}}{\partial \hat{x}_k \partial \hat{x}_k}$$

$$+\frac{\partial\left(\overline{-\hat{\theta}' \hat{u}_i'}\right)}{\partial \hat{x}_i}+\left[\frac{v_o}{u_o L_o}\right]\underbrace{\left[\frac{u_o^2}{c_{po}\left(\Delta T\right)_o}\right]}_{5}+\text{etc} \tag{11}$$

Here two additional similarity parameters result:

4. Prandtl number; $P_r = \rho_o c_{po} v_o/\kappa_o$; (12)
5. Eckert number; $E_c = u_o^2/c_{po}\left(\Delta T\right)_o$ (13)

If these two parameter criteria are satisfied then thermal similarity exists. For wind-tunnel simulation in air the Prandtl number criterion is automatically satisfied and the Eckert number criterion is only important in compressible flow which is not of interest in the present case.

Boundary conditions

In addition to matching critical non-dimensional parameters between full scale and wind tunnel, it is also necessary to make critical non-dimensional boundary conditions identical between full scale and wind tunnel. The four most important non-dimensional boundary conditions for physical modeling are: 1) the mean normalized velocity, turbulence intensity, and turbulent energy spectra profiles; 2) the roughness Reynolds number, $z_o u_*/v$; 3) Jensens length-scale criterion of z_o/H; and lastly, 4) the ratio of H/δ. Each will be briefly discussed with emphasis on practical wind-tunnel implications of each boundary-condition criterion. Snyder (1972) provides excellent discussions of these conditions.

The simulation of the approaching natural wind in the wind tunnel involves matching the non-dimensional mean velocity, turbulence intensity and energy spectra profiles. Matching the normalized mean velocity profiles involves selecting the appropriate wind-tunnel floor roughness that will produce the correct or desired value of power-law exponent, α. The power-law profile is known to reasonably describe the entire ABL (Hellman, 1916 and Davenport, 1965) and is given by the equation

$$\frac{\overline{u}}{\overline{U}_{ref}} = \left(z/z_{ref}\right)^{\overline{\alpha}} \tag{14}$$

where $\overline{U}_{ref}$ and z_{ref} are the mean speed and height of a reference location. The reference location may be any point located within the ABL; however, it is usually taken as the upper edge of the ABL such that z_{ref} is equal to δ, the ABL height, and $\overline{U}_{ref}$ if the geostrophic wind speed, Vg.

Table 1 presents the known field relation between values of $\overline{\alpha}$ and equivalent-surface-roughness height, z_o. By increasing or decreasing the wind-tunnel floor roughness, the simulation value of $\overline{\alpha}$ may be decreased or increased. With some care, the wind-tunnel

Table 1. Values of the surface roughness parameters z_o $\bar{\alpha}$

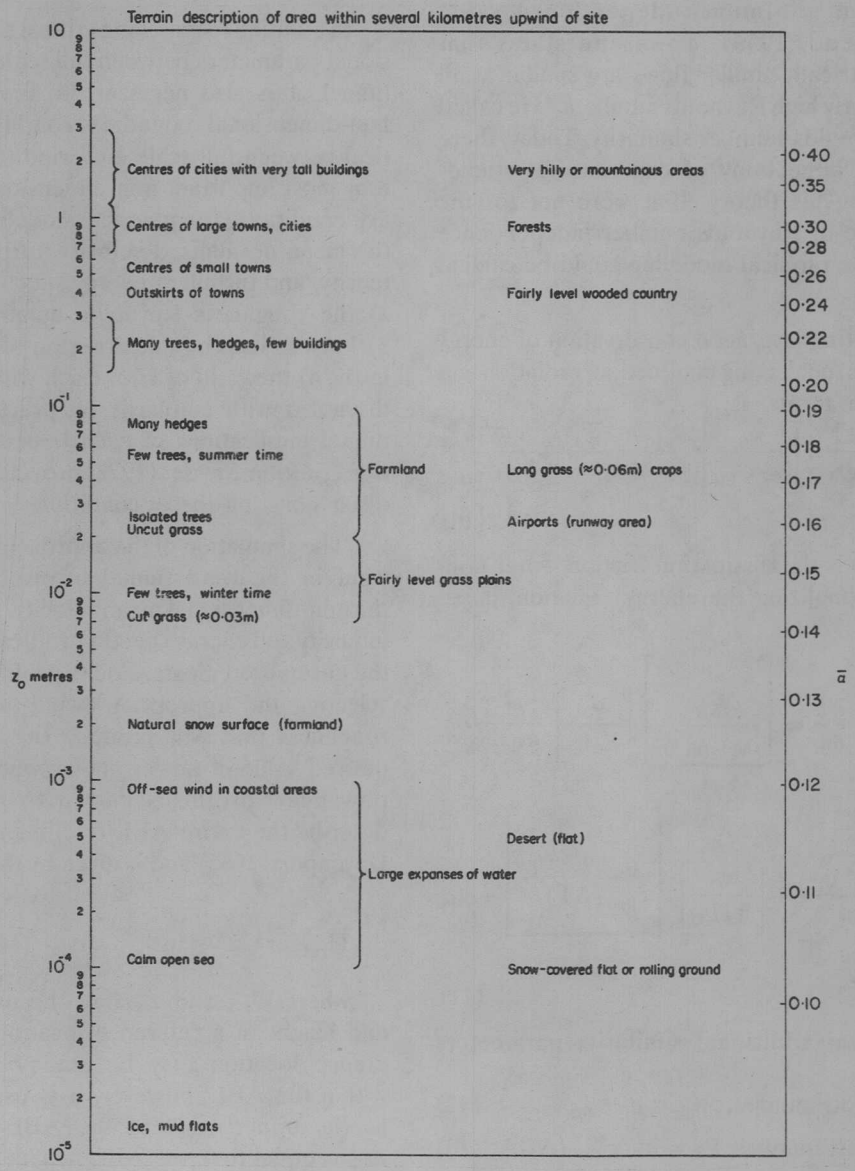

$\overline{\alpha}$ value can be made to match the full-scale $\overline{\alpha}$ value. As may be observed in Table 1, typical values of $\overline{\alpha}$ for arid-desert type conditions range from 0.09 (mud flats) to 0.12 (flat desert playa) and have a corresponding range of z_o from 10^{-5} to 10^{-3} meters, respectively.

The normalized turbulence intensity profiles should be matched in the lower portion of the wind-tunnel boundary layer to that of the ABL. Note, it is not possible to match the entire turbulence intensity in normalized profile wind-tunnel simulation due to scaling effects. The longer the flow development sec-

tion of the wind tunnel is, the better the match of normalized turbulence intensity profiles between wind-tunnel and full-scale profiles will be. The same is true for matching the inertial subrange region of the non-dimensional energy spectra profiles between the wind tunnel and ABL. The introduction of flow spires, either two- or three-dimensional, at the entrance will improve the energy spectra of the wind tunnel, possibly resulting in shorter flow development sections as compared to the wind tunnel without entrance spires present (Burke, 1982).

In wind-tunnel simulation of ABL flows, the mean non-dimensional velocity profile is easiest to match to full scale; next easiest to match are the turbulence intensity profiles, and the most difficult to simulate accurately are the energy spectra profiles. A general rule-of-thumb is that one needs 10 to 25 boundary-layer height lengths of fetch to match the mean non-dimensional velocity profile, about 50 boundary-layer height lengths to match the turbulence intensity profiles, and 100 to 500 boundary-layer height lengths to match the normalized turbulent energy spectra. As may be quickly calculated for laboratory boundary heights greater than 1 meter, excessive fetch lengths would be required, especially for matching the turbulent energy spectra. Fortunately, through the usage of spires and similar flow tripping devices, substantially shorter fetch lengths can be used to achieve a reasonable degree of simulation. Although the exact minimum fetch length for adequate simulation will vary according to the specific application, 10 to 20 meters of flow development generally suffices to meet most modeling requirements.

The second non-dimensional boundary condition that must be met in order to accurately simulate a naturally occurring ABL is for the roughness Reynolds number, $Re_r = u_* z_o/\nu$, to be greater than 2.5 (Sutton, 1949). ABL flows are almost always aerodynamically rough for which $Re_r \geq 2.5$. However, for wind-tunnel flow over smooth surfaces, the flow may not be aerodynamically rough due to the no-slip viscous flow condition at the surface. In such a case a viscous sub-layer may form on the surface. This condition is to be avoided in ABL simulation, since this situation does not exist in ABL flows. By "roughening" the surface, i.e., placing surface roughness elements on it, the flow will be "tripped" as long as the roughness elements are as large or larger than the height of the viscous sub-layer. For $Re_r > 2.5$, a Reynolds number independence is known to exist and wind-tunnel flows therefore simulate full-scale aerodynamically rough flow exactly. There is an interrelation between surface roughness, height (z_o) and velocity power-law exponent ($\bar{\alpha}$). Generally both requirements easily can be met in wind-tunnel testing.

To obtain correct simulation of the pressure distribution on objects in the atmospheric layer (i.e., dunes, etc.) in wind-tunnel modeling, Jensen (1958) observed that the surface roughness to object height ratio in the wind tunnel must be equal to that of the ABL, i.e. z_o/H in the wind-tunnel model must be equivalent to the full-scale value. Thus, the geometric scaling of the boundary condition must also be satisfied.

The last non-dimensional boundary condition that may be influential in wind-tunnel simulation is the characteristic scale height (i.e., dune height or maximum height of saltation) to boundary-layer height ratio, H/δ. If $H/\delta \geq 0.2$, then the ratio must be matched in the wind tunnel. However, if $(H/\delta)_{F.S.} < 0.2$, then only the general inequality of $(H/\delta)_{W.T.} < 0.2$ must be met (the subscript F.S. refers to the full-scale case and the subscript W.T. refers to the wind-tunnel case). The latter is generally the situation for aeolian saltation and dune simulation studies. This

principle also is stated often in reference to the law-of-the-wall logarithmic profile equation by requiring the physical model in the wind tunnel to be constrained to the lower 10 to 15% of wind-tunnel boundary-layer height. Effectively, this is the same similitude requirement only stated differently depending on whether a power-law velocity profile or law-of-the-wall velocity profile is being considered.

Other constraints

Two other constraints, not addressed in either the equations of motion analysis or boundary condition consideration, are important. First, the wind-tunnel flow should have a mean longitudinal pressure gradient of zero. This closely matches the ABL flow. Although high and low pressure systems create ABL flows, the level of pressure gradient value along the flow direction is negligible in comparison to the dynamic pressure variation due to the boundary-layer effect. The zero-pressure-gradient flow can be accomplished in the wind tunnel by having a "false" flexible ceiling that is adjustable and positioned for zero-longitudinal-pressure-gradient flow.

The second constraint is that any model (i.e., dune model, etc.) should not exceed 5 to 10% cross-sectional area blockage at any downwind location. This insures that local flow accelerations affecting the longitudinal pressure gradient will not distort the simulation flow.

It is important to note that the geostrophic wind, V_g, is not analogous to the free-stream velocity in the wind tunnel. Wind-tunnel studies are only valid for simulation of the surface layer portion of the ABL. Since this layer is essentially independent of the geostrophic wind and the Ekman spiral effect, it cannot be modeled without matching Rossby numbers. Thus, in order to simulate the entire Ekman layer, the Rossby number criterion would have to be met which would involve a rotation of the entire wind tunnel.

Simulation of Flow and Saltation Around a Dune/s

Very few scaled model experiments of saltation patterns around obstacles (i.e., dunes, etc.) in air have been performed (Tsoar, 1983). The satisfying of the Froude number is not as crucial in air as compared to water, since in air there is no pertinent free surface. Of the experiments that have been performed, most deal with the accumulation of drifting snow. In an early study by Strom *et al.* (1962) the important similitude parameters were identified as

$$D_p/L_{om}\ ,\ u^2/gD_p\ ,\ u_F/u\ ,\ e\ ,\ u_p/u$$

where L_{om} is a characteristic model length, u is the stream speed at some reference height, D_p is the particle diameter, u_F is the particle's terminal speed, e is the coefficient of restitution, and u_p is the speed of the particle.

Several important parameters of general particle saltation and sedimentation processes are presented in Table 2 (Iversen *et al.*, 1973). These parameters can be arranged to form dimensionless similitude parameters which can be used to assess some of the difficulties in modeling the full-scale conditions. Several important dimensionless parameters can be formed (Iversen *et al.*, 1973; 1975 and White *et al.*, 1975).

1. $\rho D_d/\rho_p D_p$: By varying particle density and diameter and dune length scale, this parameter can be varied from about 5,000 to 50,000 for dune lengths of 10 to 100 meters and particles from 10 μm to 1 mm. In the wind tunnel, this parameter would vary in value from about 50 to 500 for 10 cm to 1 m dunes for 10 μm to 1 mm particles. Thus, it is virtually impossible to match this important saltation parameter in wind-tunnel simulation.

Table 2. Flow and Saltation Parameters

A	Bagnold's coefficient, $u_{*_t} / \sqrt{\rho_p g D_p / \rho}$	t	Time (time)
B	Particle friction Reynolds number, $u_{*_t} D_p / \nu$	u	Velocity (length/time)
C_L	Lift coefficient, $C_L = L/(1/2\rho u^2 S_A)$	u_*	Friction speed, $\left(= \sqrt{\tau/\rho}\ \text{(length / time)}\right)$
C_D	Drag coefficient, $C_D = D/(1/2 r u^2 S_A)$	u_{*_t}	Threshold friction speed (length/time)
D	Drag, (force)	u_F	Terminal speed (length/time)
D_d	Dune diameter or characteristic length scale (length)	u_∞	Free-stream speed (length/time)
D_p	Particle diameter (length)	V_g	Geostrophic wind (above boundary layer)
e	Coefficient of restitution	x	Streamwise distance (length)
g	Acceleration of gravity (length/time^2)	y	Lateral distance (length)
h	Ripple height or reference height (length)	z	Vertical distance (length)
H	Dune height (length)	z_o	Roughness length (length)
l	Length (length)	Z'_o	Roughness length of saltation (length)
L	Reference length (length)	δ	Boundary-layer thickness (length)
		κ	von Kármáns constant
L_*	Monin-Obhokhow stability length, $L_* = u_*^3 c_p \rho T/kgH$ (length) where c_p is specific heat, T is temperature, H is heat flux at surface.	λ	Ripple wave length (length)
		μ	Absolute viscosity (mass/length-time)
R_e	Reynolds number, uL/ν	ν	Kinematic viscosity, μ/φ (length^2/time)
R_{e_r}	Roughness Reynolds number, $u_* z_o/\nu$	ρ	Mass density of atmosphere (mass/length^3)
		ρ_p	Particle density (mass/length^3)
S_A	Reference area (length^2)	τ	Shear stress (force/length^2)

2. $u(h)/u_F$: Since the threshold friction speed u_* is proportional to the reference velocity u(h), providing geometry (including roughness) is exactly modeled, the ratio of reference velocity u(h) to terminal speed u_F will be modeled exactly if the ratio u_*/u_F is satisfied and if h/L is satisfied.

3. $[u(h)]^2/gL$: The Froude number cannot easily be satisfied in the wind tunnel without having a tunnel speed far below threshold speed. Thus, it is desirable to make the wind-tunnel speed as small as possible yet still satisfy other parameters, e.g., $R_{e_r} > 2.5$. Again since u_* is proportional to u(h), this is equivalent to requiring a modeling material with as small a threshold speed, u_{*_t}, as possible. The value of this parameter varies from 0.01 to 5 in the field and from approximately 10 to 100 in the wind tunnel. Thus, wind-tunnel simulation leads to geometric distortion of erosion and depositional patterns around dunes for nearly all cases.

4. e : The coefficient of restitution is satisfied if model and atmospheric materials have equivalent elastic properties.

5. l/H : Topographic features should be scaled exactly to satisfy this criterion. At large distances upstream from the region of in-

terest, it is probably only necessary to have equivalent scaled aerodynamic roughness.

6. z_o/H : The aerodynamic roughness should, in general, be to scale (Jensen, 1958). Except for those dunes surrounded by large-scale rough surface features, this is probably small in the field. If the corresponding model surface in the wind tunnel is too smooth, it may be necessary to distort this parameter in order to meet the turbulent boundary layer requirement, $Re_r > 2.5$. It is important at the same time to insure that the ratio z_o/H also be satisfied, which is very difficult to achieve in wind tunnels.

7. z'_o/D_p : If the equivalent roughness height in saltation z'_o is proportional to particle diameter, this parameter obviously cannot be satisfied in laboratory simulations since such fine particles would have high threshold speeds. Also, if introduced into the air stream, the particles would go into suspension and the saltation process would not occur. If the equivalent roughness z'_o is proportional to u^2_F/g (Owen, 1964), then z'_o/D_d is proportional to $\rho_p D_p/\rho D_d$, the inverse of the first parameter. Thus, trying to satisfy one parameter would be at the expense of the other.

8. h/L: The reference height h at which the reference speed is measured should be located within the logarithmic portions of the wind tunnel and ABL.

9. z_o/L_*: With a "naturally" developed boundary layer in the wind tunnel, a boundary-layer velocity profile corresponds to a neutrally stratified ABL for which the Monin-Obhukov stability length L_* is infinite and the ratio z_o/L_* is zero. A finite value of L^* is achieved in the wind tunnel by heating or cooling the floor to obtain unstable or stable stratification. Another way of obtaining a nonneutral velocity profile in the wind tunnel (but perhaps not correct modeling of turbulence characteristics) would be by means of shear fences, graded grids, etc. (Counihan, 1969).

10. λ/L : The relative ripple length may be related to z'_o/L and the same comments apply as stated in item 7.

11 & 12. u_F/u_{*t} and $u_{*t}D_p/v$: As will be shown below, for a given condition such as a modeling material corresponding to minimum threshold speed, these two parameters would have the same values as for minimum threshold speed material in both the wind tunnel and field.

13. u_*/u_{*t} : The manner in which particles are transported and, in particular, the amount of material which is moved is a function of this ratio. Thus, in order to keep u_* as small as possible due to Froude number constraints, the threshold friction speed, u_{*t}, of the particle should be as small as possible.

14. u(h)t/L: The time scale in the wind tunnel is much shorter than in the field since the characteristic time is the ratio of characteristic length L to reference velocity u(h). The time necessary for pattern development in the field can thus be predicted from wind-tunnel tests.

15. A Reynolds number u(h)L/v may or may not be an important modeling parameter. For turbulent flows over sharp-edged features, the flow is relatively independent of Reynolds number. The critical model Reynolds number (above which no further changes in flow fields around objects occur with increases in the value of Reynolds number) depends upon model shape. If the model is streamlined such that the test Reynolds number is below the critical Reynolds number value, the model may have to be distorted by roughening the surface, creating sharper edges, etc. in

order to lower the critical Reynolds number. Snyder (1972) quotes critical Reynolds number for sharp-edged cubes of 11,000 and 79,000 for a hemisphere cylinder. In the current case for dunes, independence Reynolds numbers based on dune flow fields are generally about the same values for hemispherical shaped objects or about 100,000 to 500,000.

In addition to the previously mentioned criteria for similitude analysis, further discussions can be found in Strom *et al.* (1962); Warnock (1948), and Iversen *et al.* (1975 and 1976).

The physical simulation of the movement, deposition and erosion of fine particles upon a complex terrain on a smaller geometric scale presents a complicated problem. The eroding of soil or sand is an intricate function of mean wind speed, frequency and intensity of wind gusts, particle-size distribution, density and shape of particles, surface drag forces, and the geometry of the topographic features, as illustrated in the above parameter discussion. It cannot be simulated in the wind tunnel if saltation or particle movement is present.

However, the wind-flow pattern over a dune would be similar to wind patterns observed over dunes in the ABL if the dune height to surface roughness ratios in laboratory and field are the same (Sedney, 1973; Gregory and Walker, 1951; Hunt, 1971). A vortex would form around the flanks of the dune with the trailing vortices emanating downstream from the dune's two trails. The tangential component of velocity in each trailing vortex would be outward away from the wake centerline near the surface and inward above the vortex cores. The axial velocity components near the surface just behind the downstream lee area, where the flow is separated, would be minimal on the wake centerline with maximum shear stresses occurring on either side of the wake. Further downstream the two surface shear maxima merge, and the maximum shear stress in the wake would be then on the centerline.

Not all of the similitude parameters can be satisfied simultaneously in a scaled model experiment. In the case of modeling dunes, generally large geometric scaling factors are needed in order to properly simulate physical flow conditions and they simply cannot be met in the wind tunnel. The parameter D_p/L cannot be satisfied in normal simulation facilities, e.g., if D_p of a particle is 300 microns and the dune to be modeled is 100 m, then the parameter D_p/L would be 3×10^{-6}. This would mean that the particle size of a 30 cm wind-tunnel model crater would be less than one micron. Obviously such small particles are not suitable since the cohesive and interparticle forces would result in a relatively high threshold speed that when blown from the surface would go directly into suspension and therefore would not simulate the saltating phenomenon associated with the eolian process. A further complication that would result in the use of such small particles is that the threshold speed would be too high in order to satisfy other parameters, namely u^2/gD_p.

Therefore, the use of additional aides is helpful in order to determine the most important parameters or combinations of parameters of model simulation since critical similitude parameters cannot be met. One proven method used to gain additional insight into the modeling problem is the non-dimensionalization of the governing particle-flow equation of motion. Upon doing so several dimensionless parameters are manifested. After basic assumptions applied to the flow problem, the following parameters needed to be satisfied to ensure dynamic similarity (White *et al.*, 1975 and Iversen *et al.*, 1975):

$$\left[\frac{H}{z'_o}\right]_{\text{wind tunnel}} = \left[\frac{H}{z'_o}\right]_{\text{field}} \qquad (15)$$

$$\left[\frac{x}{D_d}\right]_{\text{wind tunnel}} = \left[\frac{x}{D_d}\right]_{\text{field}} \tag{16}$$

$$\left[\frac{C_D \rho D_d}{\rho_p D_p}\right]_{\text{wind tunnel}} = \left[\frac{C_D \rho D_d}{\rho_p D_p}\right]_{\text{field}} \tag{17}$$

$$\left[\frac{gD_d^2}{u_*^2 H}\right]_{\text{wind tunnel}} = \left[\frac{gD_d^2}{u_*^2 H}\right]_{\text{field}} \tag{18}$$

The satisfaction of Equation (16) is simple as it just requires geometric similarity of topographic features in the horizontal directions. Small scale bed-form features such as ripple wave-lengths would not be expected to scale without simultaneous satisfaction of all the original modeling parameters.

The satisfaction of the other three similitude parameters is more difficult. Owen (1964) has shown that the equivalent roughness height in saltation is approximately proportional to the ratio of the friction velocity squared to the gravity. Thus Equation (15) becomes

$$\frac{H}{z'_o} = \frac{2gH}{u_*^2} = \frac{2gH}{u_{*_t}^2}\left(\frac{u_{*_t}}{u_*}\right)^2 ; \tag{19}$$

however, when considering Bagnolds (1941) representation of the threshold friction velocity this equation becomes

$$\frac{H}{z'_o} = \frac{2}{A^2}\frac{\rho}{\rho_p}\frac{H}{D_p}\left(\frac{u_{*_t}}{u_*}\right)^2$$

$$= \frac{2}{A^2}\left(\frac{u_{*_t}}{u_*}\right)^2 \frac{\rho D_d}{\rho_p D_p}\left(\frac{H}{D_d}\right). \tag{20}$$

Similarly Equation (18) becomes

$$\frac{gD_d^2}{u_*^2 H} = \frac{gD_d^2}{u_{*_t}^2 H}\left(\frac{u_{*_t}}{u_*}\right)^2$$

$$= \frac{1}{A^2}\left(\frac{u_{*_t}}{u_*}\right)^2 \frac{\rho D_d}{\rho_p D_p}\left(\frac{D_d}{H}\right). \tag{21}$$

Also, the threshold parameter A is a function only of the particle friction Reynolds number B (White, 1979; Iversen and White, 1982), thus the drag coefficient may be given as:

$$C_D = \frac{4}{3A^2}\left(\frac{u_{*_t}}{u_F}\right)^2 \tag{22}$$

The parameter A is constant for larger particles and, therefore, values of A and C_D in the wind tunnel and field would be approximately equal. However, this is not true for small particles. The ratio of terminal to threshold friction speed u_F/u_{*_t} may be varied in the wind tunnel by adjusting the free-stream speed from values slightly below unity to several times unity as is also probably the case in the field. Thus, the groupings of parameters of most interest for particle flow past dunes are (White *et al.*, 1975 and Iversen *et al.*, 1975):

$$\left[\frac{1}{A^2}\left(\frac{u_{*_t}}{u_*}\right)^2 \frac{\rho D_d}{\rho_p D_p}\frac{H}{D_d}\right]_{\text{wind tunnel}} = \left[\frac{1}{A^2}\left(\frac{u_{*_t}}{u_*}\right)^2 \frac{\rho D_d}{\rho_p D_p}\frac{H}{D_d}\right]_{\text{field}} \tag{23}$$

$$\left[\frac{1}{A^2}\left(\frac{u_{*_t}}{u_F}\right)^2 \frac{\rho D_d}{\rho_p D_p}\right]_{\text{wind tunnel}} = \left[\frac{1}{A^2}\left(\frac{u_{*_t}}{u_F}\right)^2 \frac{\rho D_d}{\rho_p D_p}\right]_{\text{field}} \tag{24}$$

$$\left[\frac{1}{A^2}\left(\frac{u_{*_t}}{u_*}\right)^2 \frac{\rho D_d}{\rho_p D_p}\frac{D_d}{H}\right]_{\text{wind tunnel}} = \left[\frac{1}{A^2}\left(\frac{u_{*_t}}{u_*}\right)^2 \frac{\rho D_d}{\rho_p D_p}\frac{D_d}{H}\right]_{\text{field}} \tag{25}$$

The approximate ranges of values of the individual parameters in the wind tunnel and in the field are listed in Table 3.

Table 3. Similitude parameter values

Parameter	Field	Wind Tunnel
u_F/u_{*_t}	1 to 15	1 to 15
u_*/u_{*_t}	0.8 to 2.0	0.8 to 2.0
$\rho D_d/\rho_p D_p$	500 to 50,000	50 to 500
l/A^2	1	0.01 to 0.0001

Examining the range of values given in Table 3 it is observed that the last two critical parameters cause the similitude equations not to be satisfied. Also, in many "typically" laboratory simulations the mismatch would be large, demonstrating mathematically that it is not possible to simulate particles around dunes in the laboratory. This is a disappointing, but realistic, result.

Simulation Flow Around a Dune in the Absence of Saltation

The experimental determination of a three-dimensional turbulent boundary layer flow field in the presence of a perturbation element like a sand dune structure is one of the most formidable problems in current fluid mechanics research. The development of an analytical theory is difficult since the effects of the strong viscous interaction in the neighborhood of the perturbation must be accounted for in three dimensions. Consequently there has been little progress made in either the theoretical development or the experimental investigation.

Characteristics of the flow field

The flow around an idealized dune may be considered to be a good example of the above situation. There are two general types of disturbances that exist in the flow field. One is with a "large scale" disturbance element present which is typically larger than the surface layer height of the ABL, i.e., greater in height than about 100 m, and the second is a "small scale" disturbance element. In the case of the "small scale" element, the disturbance of the flow field is contained within the surface layer adjacent to the ground. The main difference between the large protuberance and the small one (relative to the boundary layer thickness) is that the small-scale disturbance has only a local effect on the pressure gradient; whereas, the large-scale disturbance is a non-equilibrium ABL flow.

In order to have a good conceptual understanding of three-dimensionally disturbed flows there are several common characteristics to all flows whether or not the boundary layer is laminar or turbulent and regardless of the dimensions or geometry of the protuberance element and speed of the flow. In most cases the law-of-the-wall velocity profile equation for a boundary layer flow will break in the vicinity of the protuberance; however, downstream the equation again will be valid when the effects of the disturbance have diminished. In the region of the disturbance the flow will experience streamwise vorticity (crossflow). Immediately upstream of the disturbing element one or more pairs of vortices are induced. The primary vortex stretches around the front of the disturbance (dune) and is termed a horseshoe-shaped vortex. The horseshoe vortex can be traced back to the secondary flow in the boundary layer upwind of the disturbance. A secondary set of vortices in an opposite sense of the primary pair exists on the outer side of the axial centerline next to the primary set. Another set of vortices exists behind the disturbing element. This set is comprised of closely spaced vortex filaments originating from spiral filaments which rise vertically behind the element; however, the secondary pairs of vortices are generally too weak to be easily observed or measured. These

vortex filaments are unstable and immediately breakdown to form the separated flow in the lee of the three-dimensional dune.

The height of the filaments is approximately the same height as the disturbance element, but in contrast the horseshoe vortex is located closer to the surface. The sense of rotation of the horseshoe vortex is clockwise as looking downstream from in front (upstream) of the element at the left-side vortex which extends axially downstream. Gregory and Walker (1951) were the first to explore this type of phenomenon. These vortices affect the velocity profiles of the flow by a redistribution of the momentum immediately downstream of the element. The spanwise velocity profile in such cases was studied by both Tani *et al.* (1962) and Gregory and Walker (1951). In the protuberance situation of three-dimensional flow in a boundary layer, vorticity stretching, concentration of vorticity upstream and downstream, and viscous effects must all be considered. Fig. 1 displays a drawing of a horseshoe vortex system around this type of flow disturbance.

Although data are very limited on three-dimensional flow around a disturbance there are some experimental results available that support the existence of the vortex systems. From the work of A. Hiderks, Prandtl (1952) presents pictures of flow around a disturbance exhibiting the horseshoe vortex and two symmetrical spirals immediately downstream of the disturbance. Benson (1966) also pictorially shows the vortex system's existence for a hemispherical protuberance element.

It can be said that the resulting flow fields, while complex, do exhibit characteristic vortex patterns that are not unique to the flow conditions but are widely observed for many different flows. A very perceptive statement is found in Sedney's (1973) paper, "The three-dimensional perturbations found in experimental results are so complex in the neighborhood of the protuberance that it is unlikely that an analysis can be developed that is capable of describing that part of the flow field. There is hope that progress can be made toward analyzing the downstream flow field."

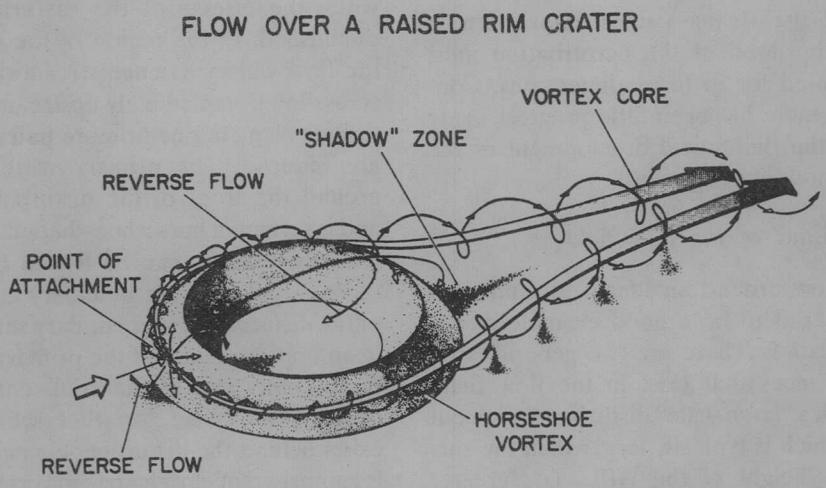

Fig. 1. Typical flow around a surface obstacle, in this case it is a raised-rim crater, showing a horseshoe vortex system. Axial velocity maxima (shown as vortex cores) of the trailing vortices converge downwind from the crater, forming a zone of higher surface stress than outside the wake.

Wind-tunnel modeling of the flowfield around small dunes and other surface structures is possible if the most important similitude parameters can be matched between field and wind tunnel. In the absence of saltation the active simulation parameters given in Table 2 decrease dramatically. The inherent problem of scaling sand-size particles, given in the case with saltation, disappears and one no longer must worry about the $\rho D_d/\rho_p D_p$ and z'_o/D_p which opposed each other in particle-flow simulation around dunes.

The simulation problem reduces to a dimensionless analysis of parameters that give the functional relationship of the pressure distribution, Δp, or force distribution (drag), D, about the dune. By performing a Buckingham's π analysis on the important flow parameters, the critical simulation parameters are determined to correctly scale the flowfield in the wind tunnel (Langhaar, 1951). The force distribution is usually presented as a differential pressure Δp which may be stated as some unknown function, f, of these variables:

$$\Delta p = f\left(\frac{D_d}{H}, \frac{L}{H}, \frac{z_o}{H}, \text{and } R_{eH}\right) \qquad (26)$$

The Euler number, Eu, is the non-dimensional force or pressure distribution that is to be duplicated in the simulation. The first two terms in the function, D_d/H and L/H, represent geometrical similarity and are matched exactly if a geometrically similar model is used. The key to the simulation lies in matching the remaining two terms, z_o/H and R_{eH}. The Reynolds number is based on a reference speed (usually taken of the dune or obstacle height in the boundary layer) and the characteristic dune height. If the model Reynolds number exceeds the independence Reynolds number then it need not match the full-scale value of field Reynolds number.

Therefore, in order to simulate flow around a dune or other surface obstacle in the laboratory the following conditions must be met: i) a geometrically similar model must be used; ii) the z_o/H ratio must be equivalent between field and laboratory; and iii) the Reynolds number value must exceed the minimum Reynolds number independence value. This is estimated to be about 100,000 to 500,000 for dune-shaped surface features, depending upon how streamlined the feature is. The more streamlined the dune the greater the Reynolds number independence value will be.

Consideration of the simulation requirements infer that large wind tunnel and higher test speeds be used in modeling (in order to achieve the independence Reynolds number value). In many cases small-scale dunes may be successfully modeled for flowfield features in the wind tunnel.

Studies on flowfield from experimental investigations of flow around various surface obstacles are given in Tsoar, White, and Berman (1995), White and Tsoar (1996) and for sand fences in White and Cho (1994).

In summary, it is possible to scale dunes for the purpose of flowfield simulation as long as the simulation Reynolds number, based on dune height, is greater than 100,000 to 500,000. This requirement usually means a relatively large-scaled model of a dune must be used to achieve such a large Reynolds number value. It is generally not possible to model larger features such as dune field or multiple dunes.

Simulation of Field Saltation

The study of saltating materials is best done in a laboratory wind tunnel. There is little, if any, compromise between field saltation and wind-tunnel saltation. Much of the fundamental understanding of saltation has come from the results of wind-tunnel studies. Starting with the remarkable work of Bagnold in the 1930s (Bagnold, 1941) many studies have been carried out defining the physics

of particle motion in saltation (Chepil, 1945, 1958 and 1959; Chepil and Woodruff, 1963; Einstein and El-Samni, 1949; Ford, 1957; Greeley and Iversen, 1981; Greeley *et al.*, 1981; Owen, 1964; White and Schultz, 1977; White, 1979, 1981, 1982, 1985, 1986a, b, 1987a, b; White and Mounla, 1991; Williams, 1963; Zingg, 1953; and many others not cited). Fundamental understanding of surface roughness effect, particle size and density, transport rates, friction speeds and effects of moisture content, interparticle force distribution and cohesion, are due to the result of laboratory wind-tunnel studies.

In the following paragraphs, a typical "saltation wind tunnel" is described and various techniques of saltation measurements are presented. The basic nature of these wind tunnels is "forgiving" in the sense that only a few basic rules of design and operation need to be followed in order to obtain high-quality data. These key ideas are discussed from a practical or implementation point-of-view. Only two major constraints govern the design and usage of saltation wind tunnels. They are: i) the tunnel requires a minimum fetch distance to allow the velocity profile to achieve an equilibrium state when saltation is present; and, ii) the internal height of the tunnel must be sufficient to meet the minimum Froude number criterion described below. Other than these two features the saltation wind-tunnel design is nearly unrestricted.

Typical wind-tunnel facility

A number of saltation experiments have been performed in a boundary-layer saltation wind tunnel located at UC Davis and is shown schematically in Fig. 2. The tunnel was designed to simulate particle flow in saltation, and it consisted of four major sections: i) entrance, ii) flow development, iii) test, and iv) diffuser. The overall length of the tunnel was 13 meters and is typical of many laboratory wind tunnels studying particle flow.

The entrance section consisted of a 0.48 m long contraction area having a ratio of 5:1 equipped with honeycomb flow-

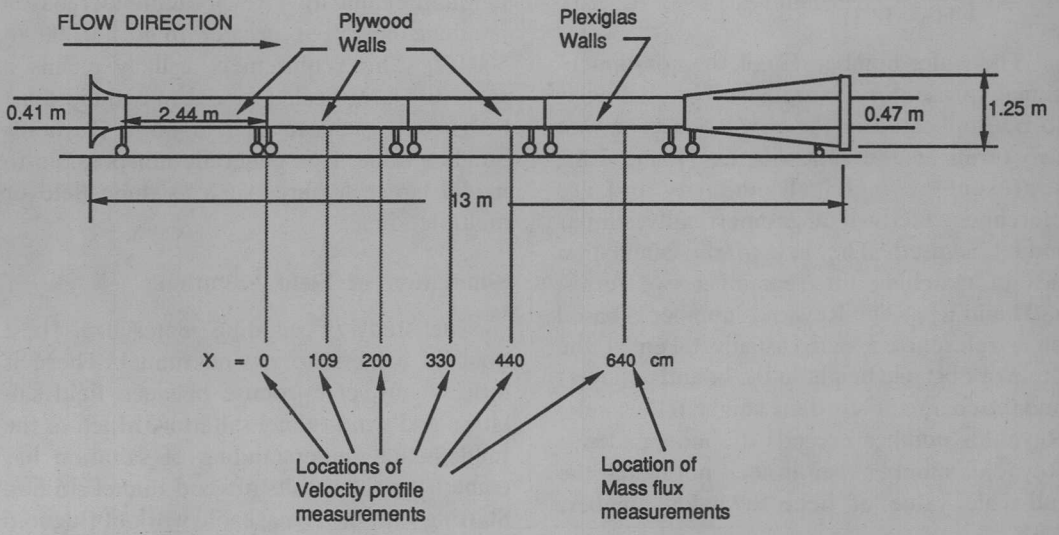

Fig. 2a. Schematic diagram of the saltation wind tunnel at the University of California, Davis.

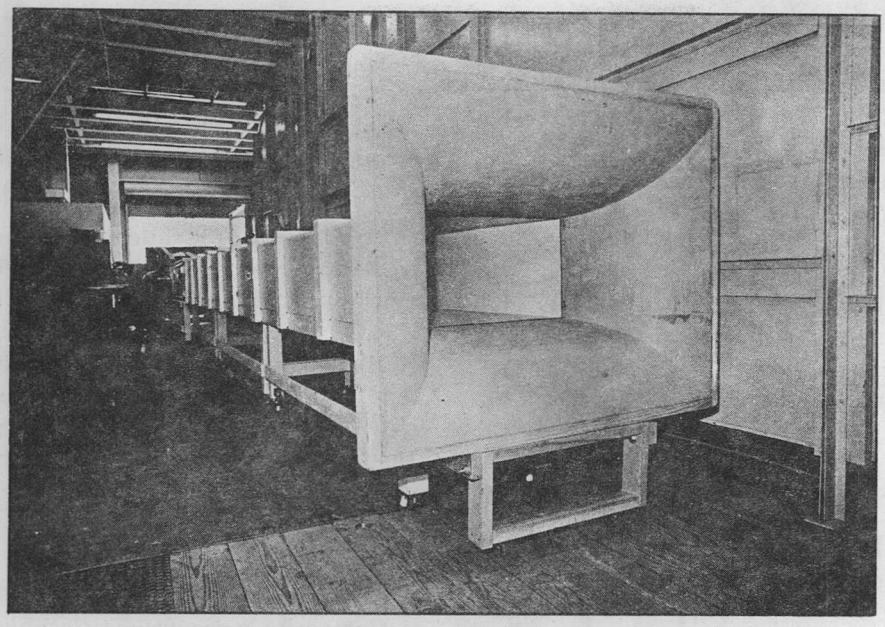

Fig. 2b. Photograph of the saltation wind tunnel located at the University of California, Davis.

straighteners to reduce the freestream turbulence level. The 7.32 m flow development section had diverging walls and was composed of three individual sections which were each

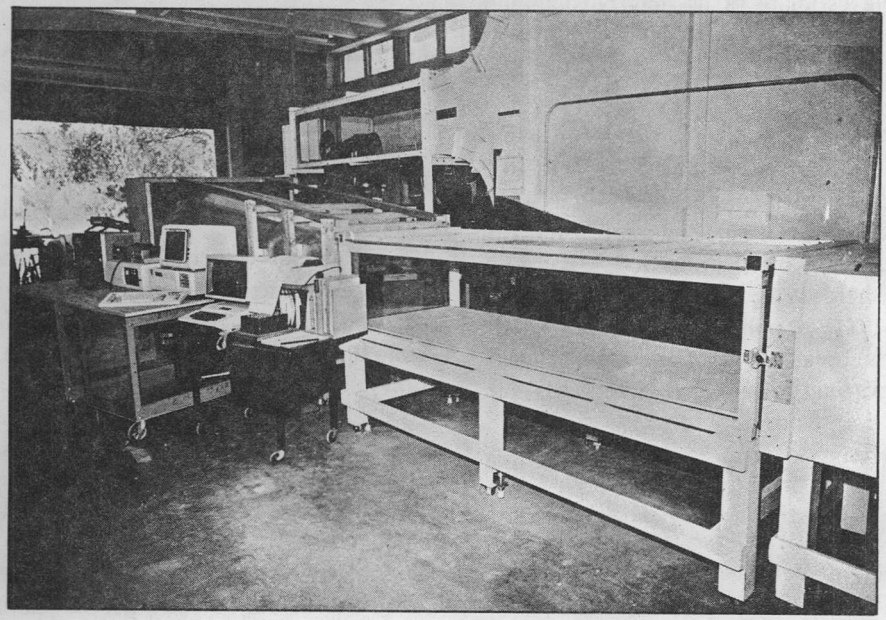

Fig. 2c. Photograph of the test section at the saltation wind tunnel.

2.44 m (8 feet) long made of plywood. The Plexiglas test section was 2.44 m in streamwise length and 0.47 m high by 0.8 m wide in cross section. The diffuser, 2.8 m in length, had an expansion area ratio of 13:1 which provided a continuous transition from the rectangular cross section of the test section to a circular cross section for the fan.

The tunnel was equipped with a 3 hp, variable speed DC motor that rotated an 8-blade fan. An AC/DC power converter supplied power to the motor, and had controllable air speed inside the tunnel of up to 20 m/s.

Saltation friction speed

The friction speed, u_*, in the presence of saltating particles, could not be determined by using the simple slope method because of the ambiguity in the velocity profile. However, when the wake region is accounted for in much the same manner as Coles' law-of-the-wake equation for smooth-wall turbulent boundary layer case (Coles, 1956), a reasonable estimate of u_* may be obtained.

The rough-wall case, with saltation occurring, may be represented by

$$\frac{u}{u_*} = \frac{1}{k} ln\,(z/z_o) + \frac{\Pi}{k}\left(1 - \cos\left(\pi\, z/\delta\right)\right) \quad (27)$$

where, k, von Kármáns constant, equals 0.418; and Π, Coles' wake parameters, is a function of pressure and momentum-deficit Reynolds number; here it is assumed equal to 0.55 (White, 1981). Applying this relation at the edge of the boundary layer and at an arbitrary location within the boundary layer yields (subtracting one from the other):

$$\frac{u_\infty - u}{u_*} = \frac{-1}{k} ln\,(z/\delta) + 1.32\,(1 + \cos\,(\pi\, z/\delta)) = F \quad (28)$$

or

$$u_\infty - u = u_* F \quad (29)$$

Note, the form of the rough-wall velocity defect, $u_\infty - u$, is essentially the same as the smooth-wall case, since the additive constant in both cases disappears when the difference of u_∞ from u is taken.

Fig. 3 presents the difference between the freestream velocity and the instantaneous velocity within the boundary layer as a function of F. The slope of this plot corresponds to the friction speed as given in Equation (29). Thus, the friction speed may be determined from the velocity profiles measured during saltation. This calculation is needed to determine the constancy of u_* with the downstream position and Froude number.

Composite mean velocity profiles in saltation

Composite mean velocity profiles were measured during saltation at different locations along the tunnel to determine the friction speed variation as a function of downstream location. To insure uniform test conditions, at the end of each previous run, the particle bed was reconditioned to its original 7.5 m length and position, by replacing particles over the eroded portion of the surface and again smoothing it. The bed length had to be maintained constant, since the variation of the friction speed as function of the downstream location is to be considered.

The mean velocity profiles (logarithmic height as a function of speed), in the presence of saltating particles, follow a straight-line from the surface and then experience a deflection point at a certain height to follow another straight line to the edge of the boundary layer. Fig. 4 displays the composite profiles (A, B, C, and D on each figure) at downstream bed positions of 1.1, 2.0, 3.3, 4.4, and 6.4 meters from the beginning of the bed. The lines plotted are linear regressions determined from the actual velocity profile data. Great care was taken to match the two segments

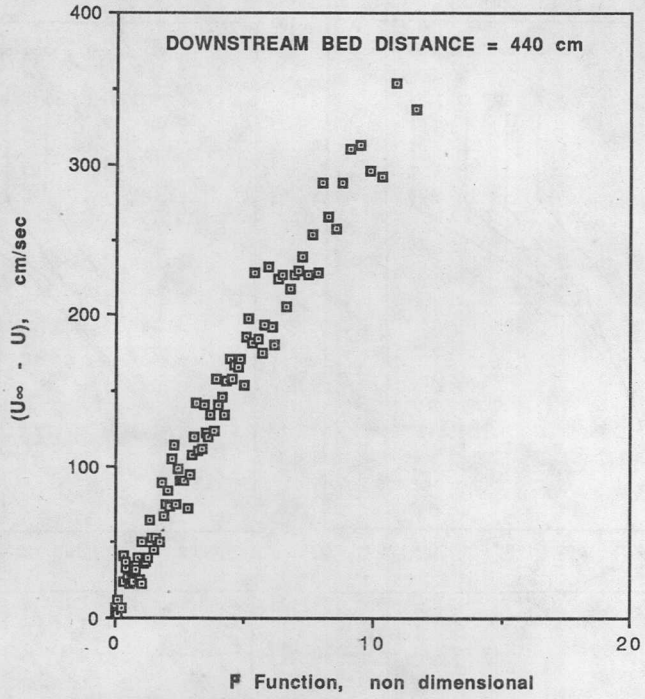

Fig. 3. The defected velocity as a function of F. The mean slope of the data is equal to the friction speed.

of each profile at their interface as well as match the local freestream speed, u_∞, above the boundary layer. The inviscid upstream velocity for each of the profiles A, B, C and D was held constant for each downstream profile measurement; note however, locally, the freestream values of the curves A, B, C and D changed as a function of downstream position. The saltating material was ground walnut shell with a density of 1.1 g/cm^3 and mean diameter of 0.25 mm. The value of the threshold friction speed for the walnut shell, at a downstream distance of 640 cm was found to be 22.5 cm/s.

Over a non-saltating rough surface, the mean velocity profiles for different speeds as functions of logarithmic height theoretically coalesce at a focus point (at zero speed) to define the roughness height z_o, as given in Equation (2). However, for a saltating flow, this focus point is shifted to finite speed, u', and a different height, k', called the roughness height in saltation (Bagnold, 1941). The speed u' is generally associated with the perceived speed at which the surface particle appears to move.

In order for this phenomenon to be measured, the saltation process must have reached an equilibrium condition, i.e., constancy of u_* as a function of downstream position. The composite velocity profile of Fig. 4 displays this u' - k' phenomenon. At a downstream distance of 640 cm from the beginning of the bed, an easily observed u' of 187 cm/s and k' of 0.22 cm are seen. These values k' of and u' compared reasonably well with the data published by Bagnold (u' = 250 cm/s and k' = 0.30 cm) and Zingg

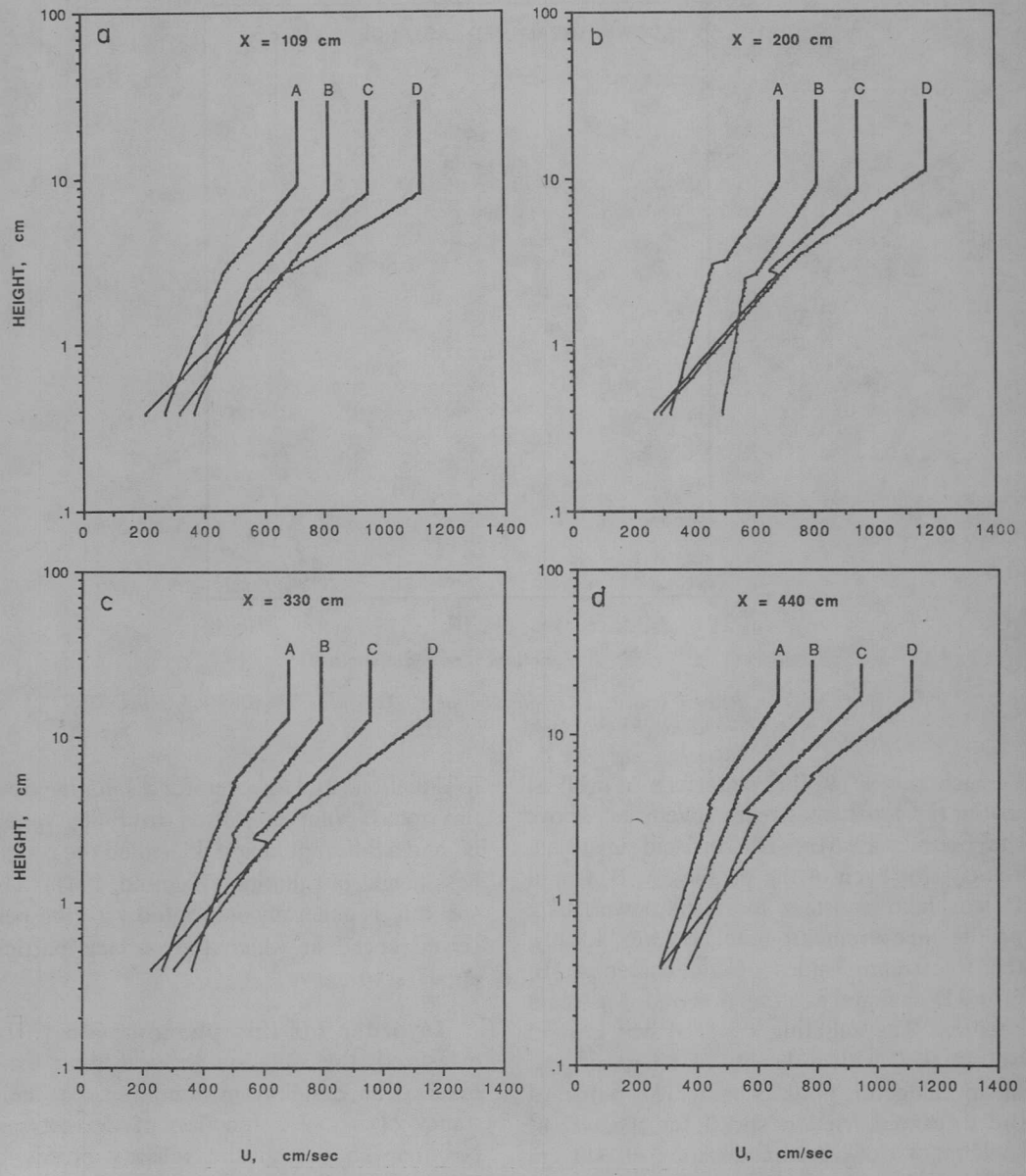

Fig. 4. Composite velocity profiles as a function of logarithmic height at downstream position of x. The solid straight lines are obtained from linear regression analyses of data. The feature of two linear portions of curve is common in wind-tunnel velocity profiles. The lower linear portion is the correct one to use for friction speed determination as it is the internal boundary layer representative of wall characteristics; Fig. 4a. Composite velocity profiles at x = 109 cm; Fig. 4b. Composite velocity profiles at x = 200 cm; Fig. 4c. Composite velocity profiles at x = 330 cm; and Fig. 4d. Composite velocity profiles at x = 440 cm.

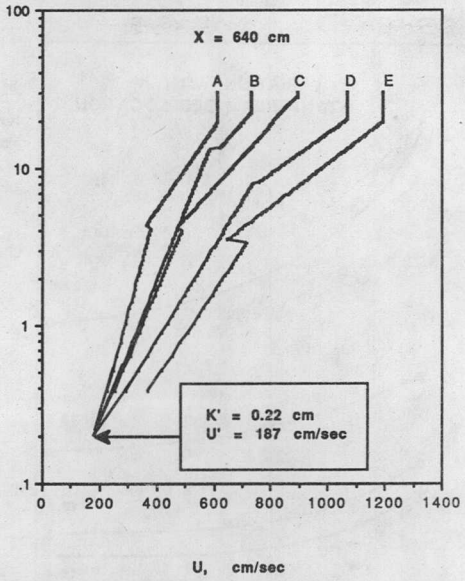

Fig. 4e. Composite velocity profiles at x = 640 cm.

(1953) who reported k′ = 10d and u′ = 895d, where d is the diameter of the mean particle in mm and k′ and u′ are expressed in cm, or for the present case u′ = 224 cm/s and k′ = 0.25 cm. Bagnold's mean particle diameter was about 20 microns, while the diameter of the present experiments was 250 microns.

Froude number effect

The Froude number is defined by the inviscid velocity upstream of the bed and is given as $Fr = u^2_\infty/(gH)$. Owen and Gillette (1985) determined that if the saltation value of Froude number is too high the saltation will be affected adversely by the wind tunnel, i.e., particles hitting the ceiling, and disturbance in pressure.

The experiments of White and Mounla (1991) have Froude numbers that range from 10.4 to 27.6, some of which are below the minimum independence number of 20 set by Owen and Gillette. Considering u_* as a function of downwind distance suggests that the u_* curves are approaching a constancy value. The smaller the value of Froude number the more rapidly the constancy of u_* is approached. In the cases where the Froude number was less than 20, it took a minimum x/H distance of at least 5 for the u_* curves to become relatively constant with further changes in downstream position.

The air flow that enters the wind tunnel is initially almost uniform. There is a minimum entrance length required for the velocity-defected layer to resemble a boundary-layer profile. Spires and other boundary layer tripping devices can shorten this entrance length; nonetheless, some minimum length still will be required to obtain a boundary layer velocity profile. The observed minimum x/H value of 5 in the current data illustrates, experimentally, the requirement of this minimum entrance length. For downstream locations less than 5H, the friction speed has not reached its steady-state value. Consequently, the saltation process has not achieved equilibrium.

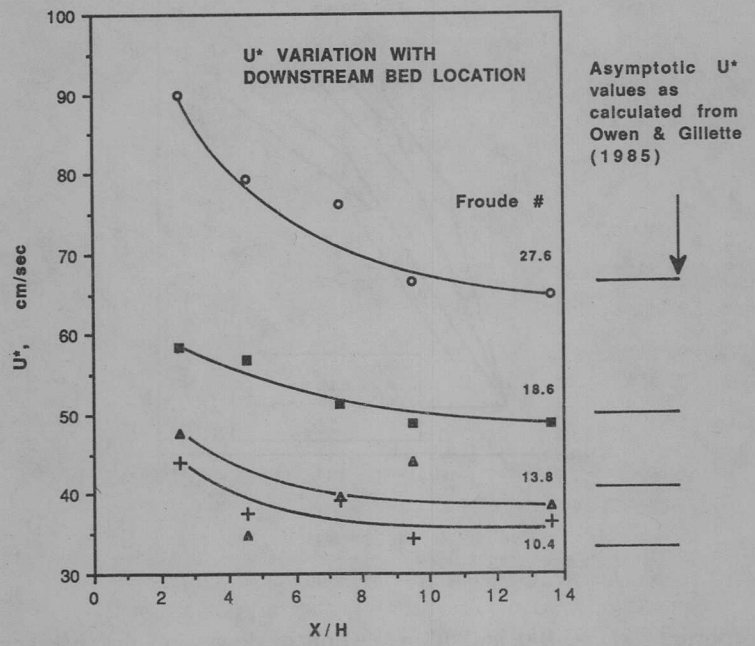

Fig. 5. The friction speed as a function of non-dimensional downstream length, x/H. Also shown, to the right of the figure, are the predicted values of Owen and Gillette, 1985, as the downstream distance becomes large. Curves A, B, C and D are for the same data as Figures 4a to 4e with Froude number values 10.4, 13.8, 18.6 and 27.6, respectively.

Perhaps a more refined measure, instead of x/H, would be x/δ, where δ is the boundary layer height. Generally, an absolute minimum of 25 is required to produce an equilibrium profile (White, 1981) and illustrated in Fig. 5. Values of x/δ from 50 to 500 are further required to insure an equilibrium flow exists in the more subtle indictors such as turbulence intensities, development of inertial subrange and energy spectra. Fortunately, these more stringent guidelines do not apply directly to saltating flows since the particle motion severely modifies the boundary layer. Nonetheless, 25δ as a minimum entrance length requirement, should be adhered to in order to establish equilibrium (constant friction speed) saltation flows. This assumes the Froude number is less than the critical value.

Mass transport

The distribution of mass flux as function of height also was measured. The particle collection system consisted of 25 individual 2 cm high, stackable Plexiglas collectors as described in White (1982) and shown in Fig. 6. Each collector had approximately a 2 cm^2 frontal cross-sectional area and a wire mesh at the back wall which allowed air and mean-sized particles of 40 microns diameter or less to pass through. The air flow through the rear-wall area of the collectors prevented separation from occurring off the sharp-edged intersection of the side wall with the rear wall. Flow visualization studies showed particles to be efficiently trapped. Once the collectors were positioned inside the tunnel and the freestream wind speed was achieved, an

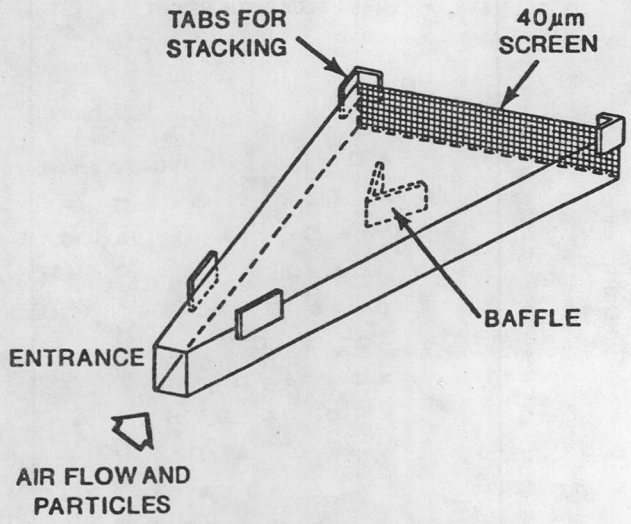

Fig. 6. Diagram of particle collector used to determine flux; collector is made of Plexiglas. Wind tunnel smoke tests were carried out by the author in the late 1970s to determine optimum angle for the wedge which would allow maximum efficiency for particle collection with minimum interference to air flow. Baffle prevents particles from bounding back out the front or damaging the screen. Tabs on the side enable collectors to be stacked.

automated collection system commenced. The length of the time for calculation of flux rates was performed by a stop watch with an accuracy of 0.01 seconds. This introduced a negligible uncertainty since collections' times were typically greater than 30 seconds. After the particles were caught in the individual traps, the material of each trap was weighed on a Metler scale (accuracy of 0.1 g).

The mass flux as a function of height was measured at a downstream distance of 640 cm; simultaneous measurements of velocity profiles also were performed at the same location. The logarithm of the mass flux was plotted as a function of the height of each collector as shown in Fig. 7. This plot should be expected to trace a straight line, as previous work has shown an exponential dependence of mass distribution with height (White, 1981 and others). At higher speeds, the appearance of a linear logarithmic relation is better than it is at lower speeds. This could be attributed to the accuracy of the scale used to measure the mass collected for a particular run. Also, at lower speeds, the uncertainty in the measurements becomes large since the collected mass is small.

Nalpanis (1985) proposed that the following relationship be used to describe the exponential dependence of mass distribution with height:

$$q = \alpha\, e^{-\left[\lambda g y / u_*^2\right]} \tag{30}$$

where, α and λ are constants for a single experiment. However, Nalpanis concluded based upon analysis of his data that "there does not seem to be any *a priori* way of determining the values of α and λ." The present data also were fitted to this expression,

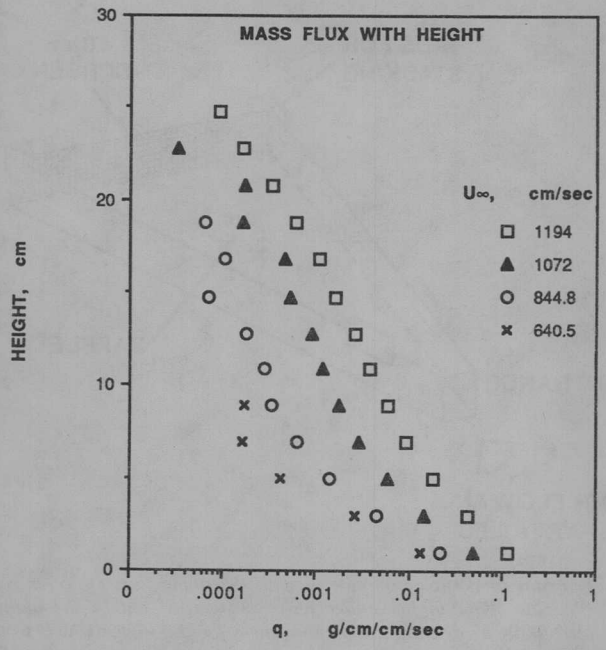

Fig. 7 The logarithm of the mass flux, q, as a function of height for different wind strengths.

and, although there are definite tendencies of the data, i.e., λ and α both increasing with increasing u_* values, the same conclusion as Nalpanis was reached for the present data. No satisfying equation could be established to account for the α and λ variation from one experiment to another. The α and λ parameters appear not to be constants but rather functions of u_*, particle density and probably functions of particle shape, distribution of particle size and surface roughness. The present values of α ranged from about 30 to 100 mg/cm^2/s, while values of λ varied from unity to about 1.5, both of which uniformly increased with increasing friction speed. The range of α and λ values somewhat agree with the Nalpanis values when the density ratio of walnut shell to sand is accounted for in the λ parameter (our λ's typically are larger by a factor of 2.5 to 3, the ratio of sand to walnut shell density).

Concluding Remarks

In the text of this paper the fundamental philosophy of laboratory modeling of saltation and wind flow around dunes has been examined. The basic nature of the ABL and surface layer, in which all of these processes take place, was thoroughly discussed to provide the necessary understanding of the underlying physics of the field processes. The general philosophy of physical modeling of atmospheric flow also was presented with special emphasis on wind-tunnel simulation techniques. The governing equations of motion were analyzed for application of laboratory testing. Key similitude parameters such as Reynolds and Froude numbers, as applied to wind-tunnel requirements, were discussed. Prevalent boundary conditions were identified and discussed in detail.

Three areas of modeling were examined: i) wind flow past a large-scale dune and/or dune fields with saltation present; ii) wind flow in the absence of saltation, around small-scale dunes and within specific areas of dunes; and iii) the general process of saltation.

The analysis of the simulating flow past large-scale surface features was disappointing as it was determined that it is not generally possible to model in the laboratory (i.e., wind tunnel). This was primarily due to the fundamental problem of scaling, which is especially severe for the combination of saltation and flow past large-scale dunes. For determination of the large-scale flow field features in the absence of saltation, only general gross wind-flow patterns are able to be determined from the simulation.

However, for the simulation of small-scale features such as limited areas of dunes or small dunes (only a few meters in length or less) the findings were more satisfying. Here dune fields could be reasonably modeled if care is taken to ensure that the minimum independence Reynolds number criterion was met in the wind tunnel as well as meeting the Jensen criterion.

Lastly, the true forte of wind-tunnel applications lies in the study of saltation. In effect, there is little compromise on the physical process of saltation occurring in the wind tunnel. This is due to the fact that saltation is not scaled but simply replicated in the tunnel. Only a few basic similitude rules need be followed to produce a high-quality saltation flow in the wind tunnel.

In conclusion the usage of wind tunnels in studying saltation and dunes is far from over. There are many experiments with significant and lasting results yet to be performed and awaiting to be conducted.

Acknowledgments

I am indebted to Ms. Lucy Day for her excellent word processing of this manuscript.

References

Arya, S.P.S. and Plate, E.J. 1969. Modeling of the stably stratified atmospheric boundary layer. *Journal of Atmospheric Sciences* 26(4): 656-665.

Bagnold, R.A. 1941. *The Physics of Blown Sand and Desert Dunes*. Methuen, London.

Benson, B.W. 1966. Cavitation inception on three-dimensional roughness elements, David Taylor Model Basin. Washington, DC, Report 2104, pp. 265.

Burke, J.P. 1982. A wind-tunnel study of low-speed turbulent boundary layer flow over a rough-to-smooth transition with and without two-dimensional vortex generators (spires). Master of Science Thesis, University of California, Davis.

Calder, K.L. 1966. Concerning the similarity theory of A.S. Monin and A.M. Obukhov for the turbulent structure of thermally stratified surface layer of the atmosphere. *Quarterly Journal of the Royal Meteorological Society* 92(301): 141-146.

Caldwell, C.W. 1972. A laboratory study of the turbulent Ekman layer. *Geophysical Fluid Dynamics* 3: 125-160.

Cermak, J.E. 1971. Laboratory simulation of the atmospheric boundary layer. *AIAA Journal* 9(9): 1746-1754.

Cermak, J.E., Sandborn, V.A., Plate, E.J., Binder, G.H., Chuang, H., Meroney, R.N. and Ito, S. 1966. Simulation of atmospheric motion by wind tunnel flows. Fluid Dynamics and Diffusion Lab, Colorado State University, *Technical Report* CER66JEC-VAS-EJP-GJB-HC-RNM-SI17.

Chepil, W.S. 1945. Dynamics of wind erosion, II: Initiation of soil movement. *Soil Science* 60: 397-411.

Chepil W.S. 1958. The use of evenly spaced hemispheres to evaluate aerodynamic forces on a soil surface. *Transactions, American Geophysical Union* 39(3): 397-403.

Chepil, W.S. 1959. Equilibrium of soil grains at the threshold of movement by wind. *Soil Science Society Proceedings*, pp. 422-428.

Chepil, W.S. and Woodruff, N.P. 1963. The physics of wind erosion and its control. *Advances in Agronomy* 15: 211-302.

Clauser, F.H. 1956. The turbulent boundary layer. *Advances in Applied Mechanics* 4: 1-51.

Coles, D. 1956. The law of the wake in turbulent boundary layer. *Journal of Fluid Mechanics* 1: 191-226.

Counihan, C. 1969. An improved method of simulating an atmospheric boundary layer in a wind tunnel. *Atmospheric Environment* 3: 197-214.

Davenport, A.G. 1965. The relationship of wind structure to wind loading. In *Proceedings of the Symposium on Wind Effects on Buildings and Structures*, Vol. 1, pp. 53-102. National Physical Laboratory, Teddington, U.K., Her Majesty's Stationery Office, London.

Einstein, H.A. and El-Samni, E. 1949. Hydrodynamic forces on a rough wall. *Reviews of Modern Physics* 21(3): 520-524.

Ekman, V.W. 1905. On the influence of the earth's rotation on ocean-currents. *Arkiv För Matematik, Astronomi Och Fysik* 2(11): 1-52.

Ford, E.F. 1957. The transport of sand by wind. *Transactions of the American Geophysical Union* 38: 171-174.

Greeley, R. and Iversen, J.D. 1981. *Wind as a Geologic Process on Earth, Mars, Venus, and Titan*. Cambridge University Press, Cambridge, pp. 100.

Greeley, R., White, B.R., Pollack, J.B., Iversen, J.D., and Leach R.N. 1981. Dust storms on Mars: considerations and simulations. In *Desert Dust: Origin, Characteristics and Effect on Man* (Ed. T. Pewe), Special Issue of Geological Society of America.

Gregory, N. and Walker, W. 1951. The effect of transition of isolated surface excrescences in the boundary layer. *Reports and Memoranda* No. 2779, Aeronautical Research Council, Great Britain.

Halitsky, J. 1969. Validation of scaling procedures for wind tunnel model testing diffusion near buildings. Geophysical Sciences Laboratory, New York University, *Technical Report* 69-8.

Hellman, G. 1916. Über die bewegung der luft in den understen schichten der atmosphäre. *Meterol. Z.* 34: 273.

Hidy, G.M. 1966. *On Atmospheric Simulation: A Colloquium*. National Center for Atmospheric Research, Boulder, CO., NCAR-TN-22.

Howroyd, G.C. and Slawson, P.R. 1975. The characteristics of a laboratory produced turbulent Ekman layer. *Boundary Layer Meteorology* 8: 201-219.

Hunt, J.C.R. 1971. The effect of single building and structures. *Philosophical Transactions of the Royal Society of London*, Series A 269: 457-468.

Iversen, J.D. and White, B.R. 1982. Saltation threshold on Earth, Mars and Venus. *Sedimentology 29: 111-119.*

Iversen, J.D., Greeley, R., Pollack, J.D. and White, B.R. 1973. Simulation of Martian eolian phenomena in the atmospheric wind tunnel. *7th Conference on Space Simulation* NASA SP-336: 191-213.

Iversen, J.D., Greeley, R., White, B.R. and Pollack, J.B. 1975. Eolian erosion on the Martian surface, Part I: Erosion rate similitude. *Icarus* 26(3): 321-331.

Iversen, J.D., Greeley, R., White, B.R. and Pollack, J.B. 1976. Saltation threshold on Mars: the effect of interparticle force, surface roughness, and low atmospheric density. *Icarus* 29(3): 381-392.

Jensen, J. 1958. The model-law for phenomena in natural wind. *Ingeniøren* 2: 121-128.

Langhaar, H.L. 1951. *Dimensional Analysis and Theory of Models*. John Wiley & Sons, New York.

Lumley, J.L. and Panofsky, H.A. 1964. *The Structure of Atmospheric Turbulence*. Wiley, New York.

McVehil, G.E., Ludwig, G.R. and Sundaram, T.R. 1967. On the feasibility of modeling small scale atmospheric motion. Cornell Aeronautical Laboratory, Buffalo, NY, CAL, Report ZB-2328-P-1.

Monin, A.S. 1970. The atmospheric boundary layer. *Annual Reviews of Fluid Mechanics* pp. 225-250.

Monin, A.S. and Obukhov, A.M. 1954. Basic regularity in turbulent mixing in the surface layer of the atmosphere. *Izv. Akad. Nauk. SSSR, Ser. Geotiz*, no. 24.

Monin, A.S. and Yaglom, A.M. 1965. *Statistical Hydromechanics*, Part I: *The Mechanics of Turbulence*. MIT Press, Cambridge, MA.

Nalpanis, P. 1985. Saltating and suspended particles over flat and sloping surfaces. II. Experiments and numerical simulation. In: *Proceedings of International Workshop on the Physics of Blown Sand*, Vol. I, pp. 37-66. University of Aarhus.

Nikuradse, J. 1932. Gesetzmä igkeit der turbulenten strömung in glatten rohren. *Forsch. Arb. Ing.-Wes.*, No. 356.

Nikuradse, J. 1933. Strömungsgesetze in rauhen rohren. *Forsch. Arb. Ing.-Wes.* No. 361.

Owen, P.R. 1964. Saltation of uniform grains in air. *Journal of Fluid Mechanics* 20: 225-242.

Owen, P.R. and Gillette, D. 1985. Wind tunnel constraint on saltation. In: *Proceedings of International Workshop on the Physics of Blown Sand,* Vol. 2, pp. 253-269. University of Aarhus.

Plate, E.J. and Ouraishi, A.A. 1965. Modeling velocity distributions inside and above tall crops. *Journal of Applied Meteorology* 4(3): 400-408.

Prandtl, L. 1952. *Essentials of Fluid Dynamics*. Hafner Publishing Co., pp. 321.

Schlichting, H. 1968. *Boundary Layer Theory*. McGraw-Hill, NY, pp. 747.

Sedney, R. 1973. A survey of the effects of small protuberances on boundary-layer flow. *AIAA Journal* 11: 782-792.

Snyder, W. 1972. Similarity criteria for the application of fluid models to the study of air pollution meteorology. *Boundary Layer Meteorology* 3: 113-134.

Strom, G.H., Kelley, G.R., Keitz, E.L. and Weiss, R.F. 1962. Scale model studies on snow drifting. R. R. 73, U.S. Army Snow Ice and Permafrost Research Establishment, Corps of Engineers, Department of Army Task, 8X99-27-001-03.

Sutton, O.G. 1949. *Atmospheric Turbulence*. Methuen, London.

Sutton, O.G. 1953. *Micrometeorology*. McGraw-Hill, NY.

Tani, I., Komoda, H., Komatsu, Y. and Iuchi, M. 1962. Boundary-layer transition by isolated roughness. Aeronautical Research Institute, University of Tokyo, *Report* No. 375, 28(7): 129-142.

Tennekes, H. 1973. The logarithmic wind profile. *Journal of Atmospheric Science* 30: 234-238.

Townsend, A.A. 1956. *The Structure of Turbulent Shear Flow*. Cambridge University Press, Cambridge, England.

Tsoar, H. 1983. Wind tunnel modeling of echo and climbing dunes. In: *Eolian Sediments Processes: Developments in Sedimentology* (Eds. M.E. Brookfield and T.S. Ahlbrandt), pp. 247-259. Elsevier Science Publishers, Amsterdam, The Netherlands.

Tsoar, H., White, B.R. and Berman, E. 1996. The effect of slopes on sand transport: numerical modelling. In: *Landscape and Urban Planning*, in press. Elsevier Science Publishers, Amsterdam, The Netherlands.

Warnock, H. 1948. *Engineering Hydraulics*. Wiley, NY.

White, B.R. 1979. Soil transport by winds on Mars. *Journal of Geophysical Research* 84(B8): 4643-4651.

White, B.R. 1981. Low-Reynolds-number turbulent boundary layers. *Journal of Fluid Engineering* 103: 624-630.

White, B.R. 1982. Two-phase measurement of saltating turbulent boundary layer flow. *International Journal of Multiphase Flow* 5: 459-473.

White, B.R. 1986a. Particle dynamics in two-phase flows. In: *Encyclopedia of Fluid Dynamics*, pp. 239-282. Gulf Publishing Co., Houston, TX.

White, B.R. 1986b. Particle transport by atmospheric winds on Venus: An experimental wind tunnel study. In: *Aeolian Geomorphology, The Binghamton Symposia in Geomorphology* (Ed. W.G. Nickling), pp. 57-74. International Series, No. 17, Allen and Unwin Publishers, Inc., Boston.

White, B.R. 1987a. A low-density boundary-layer wind tunnel facility. *AIAA Paper* 87-0291, AIAA 25th Aerospace Science Meeting, Reno, Nevada, USA.

White, B.R. 1987b. Saltation threshold experiments conducted under reduced gravity condition. *AIAA Paper* 87-0621, AIAA 25th Aerospace Science Meeting, Reno, Nevada, USA.

White, B.R. and Cho, H.M. 1996. Wind tunnel simulation of sand fences on Owens (dry) Lake, California. *Final Report* to California State Lands Commission Contract C9464, September.

White, B.R., Greeley, R., Iversen, J.D. and Pollack, J.B. 1975. Particle motion in atmospheric boundary layers of Mars and Earth. *NASA Technical Memorandum* X-62,463.

White, B.R. and Schulz, J.C. 1977. Magnus effect in saltation. *Journal of Fluid Mechanics* 81(3): 497-512.

White, B.R. and Tsoar, H. 1996. Slope effect on saltation over a climbing dune. *Geomorphology* in press.

Williams, G. 1963. Some aspects of the eolian saltation load. *Sedimentology* 3: 257-287.

Zingg, A.W. 1953. Wind tunnel studies of the movement of sedimentary material. *Proceedings of the 5th Hydraulic Conference, Bulletin* 24: 111-135.